Modification of Marcatili's Method for the Calculation of Anisotropic Rectangular Dielectric Waveguides

Sergey N. Dudorov, Dmitri V. Lioubtchenko, and Antti V. Räisänen

***Abstract*—Marcatili's method for the calculation of rectangular dielectric rod waveguides has been modified for uniaxial anisotropic dielectric materials. The averaging method without guessing the field distribution has been used to derive the equations. Experimental results for an anisotropic sapphire waveguide show a good agreement with those calculated using the approach developed here.**

***Index Terms*—Marcatili's method, rectangular dielectric waveguide, uniaxial anisotropic sapphire waveguide.**

I. Introduction

The problem of calculating the propagation characteristics of a circular dielectric waveguide can be rigorously solved relatively easily using Bessel functions. However, in the case of a rectangular dielectric rod waveguide (DRW), the problem becomes somewhat complicated, particularly when the ratio of the permittivities of the rod and that of its environment is large. The main cause of slow convergence of numerical methods is the presence of sharp corners of the DRW [1].

A good exposition of the numerical methods for calculating general millimeter-wave structures can be found, for example, in [2]. Numerous methods of this kind can be applied to the problem of rectangular DRW structures, particularly to the open rectangular DRW.

Today, the uniaxial anisotropic DRW is of increasing interest. A simple theoretical approximation model for the calculation of the propagation constant is required in addition to complicated, but accurate ones (see, e.g., [3]). The most popular approximation is the well-known "Marcatili method" [4]. However, this method was developed for isotropic materials. In this paper, a new approach to the solution of the uniaxial anisotropic case, displaying good accuracy despite its simplicity, is proposed.

II. Formulation of the Problem and Experiment

The principal focus is the case in which the optical axis of material coincides with the axis of a DRW in order to avoid the excitation of an orthogonal mode and/or rotation of the polarization plane. The E_{11}^{y} fundamental mode of the rectangular DRW with cross section $a \times b$ has been selected and, by using its symmetry, one can formulate the problem, as shown in Fig. 1.

However, rather than using the above approach, it was found in [5] that Marcatili's method for a rectangular DRW with cross section $a \times b$ involves the solution of two problems for two dielectric slabs: a horizontal slab of thickness b and a vertical slab of thickness a for the same polarization. We have used the combination of these two approaches (see Fig. 2 for the horizontal slab). In this study, we derive, using the averaging method [6], the dispersion equation for a rectangular uniaxial anisotropic DRW in the most interesting case in which the optical axis coincides with the z-axis of the DRW. This method allows one to derive the dispersion equations without guessing the field distribution.

Experiments were carried out in order to verify the calculated numerical results. Sapphire was selected as a material for DRW because it is a typical example of a uniaxial anisotropic dielectric. Sapphire is a nonmagnetic dielectric, therefore, its μ is equal to that of vacuum. S-parameter measurements of a sapphire DRW were carried out with vector network analyzer (VNA) HP 8510 using the direct connection of the input and output as a reference. A monocrystalline sapphire DRW, oriented along the optical axis, with a cross section of $1.0 \times 0.5\ \text{mm}^2$, a total length of 112 mm, and a tapering section length of 6 mm (Fig. 3) was used for the vector measurements [7]. Experiments and simulations have shown that, in the case of a nonsymmetrical tapering of the DRW end, matching is best achieved when the tip is located on the axis of the metal waveguide. This results in an experimental setup, as shown in Fig. 3.

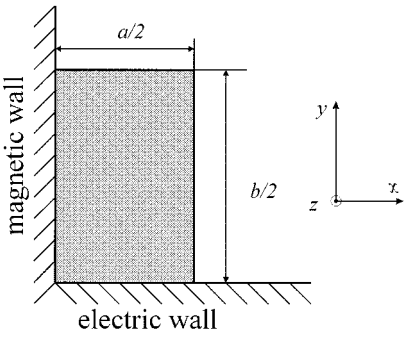

Fig. 1. Cross section of the waveguide problem.

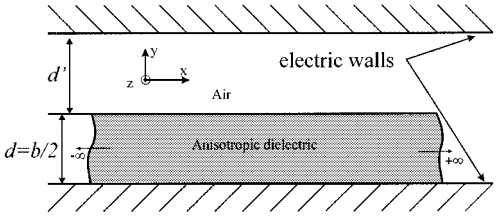

Fig. 2. Anisotropic dielectric slab waveguide problem.

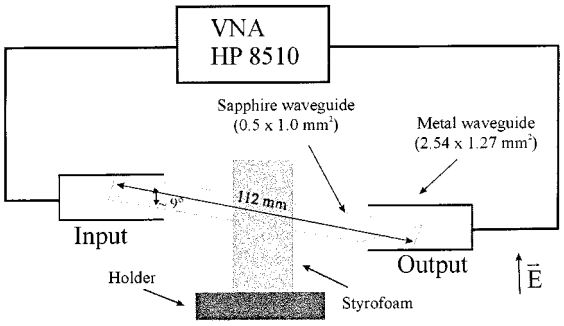

Fig. 3. Schematic setup of DWR vector measurements.

III. Theory

One can show that there is no longitudinal component E_z, only H_z, in the case of the vertical dielectric slab for the E_1^y mode, owing to $(\partial/\partial y) = 0$ and $H_y = 0$ [8]. Thus, only the E_y-component is present, and the corresponding equation in Marcatili's method does not need to be changed.

Manuscript received March 11, 2001.

The authors are with the MilliLab, Radio Laboratory, Helsinki University of Technology, Espoo FIN-02015 HUT, Finland (e-mail: sdudorov@cc.hut.fi).

Publisher Item Identifier S 0018-9480(02)05214-6.

Let us solve the dielectric slab problem shown in Fig. 2, when the dielectric permittivity is determined by the matrix

$$\varepsilon = \begin{pmatrix} \varepsilon_\perp & 0 & 0 \\ 0 & \varepsilon_\perp & 0 \\ 0 & 0 & \varepsilon_\parallel \end{pmatrix} \tag{1}$$

where $\varepsilon_\perp = \varepsilon_{r\perp}\varepsilon_0$ denotes the permittivity in the direction normal to the optical axis and $\varepsilon_\parallel = \varepsilon_{r\parallel}\varepsilon_0$ denotes the permittivity parallel to the optical axis. In the following, permeability μ is assumed to be scalar.

The main equations derived from [6] are

$$\begin{aligned} \frac{\mathbf{n}\times\mathbf{E}_{t+} - \mathbf{n}\times\mathbf{E}_{t-}}{d} &= -j\omega\mu\hat{\mathbf{H}}_t - \frac{1}{j\omega\varepsilon_\perp}\nabla_t\times\nabla_t\times\hat{\mathbf{H}}_t \\ \frac{\mathbf{n}\times\mathbf{H}_{t+} - \mathbf{n}\times\mathbf{H}_{t-}}{d} &= -j\omega\varepsilon_\parallel\hat{\mathbf{E}}_t - \frac{1}{j\omega\mu}\nabla_t\times\nabla_t\times\hat{\mathbf{E}}_t \end{aligned} \tag{2}$$

where

$$\begin{aligned} \hat{\mathbf{E}}_t &= (\mathbf{E}_{t+} + \mathbf{E}_{t-})f(\beta_y d) \\ \hat{\mathbf{H}}_t &= (\mathbf{H}_{t+} + \mathbf{H}_{t-})f(\beta_y d) \\ f(\beta_y d) &= \frac{\tan\left(\dfrac{\beta_y d}{2}\right)}{\beta_y d}. \end{aligned}$$

It is assumed that the permeability μ of sapphire coincides with that in vacuum. The transversal propagation constant β_y will be determined later. Subscript indexes $t+$ and $t-$ refer to the tangential components of the corresponding vector on the upper and lower sides of the slab, respectively. In our case, $\mathbf{E}_{t-} = 0$ because of the presence of the electric wall.

The two Helmholtz equations for the E_z- and H_z-components in a uniaxial anisotropic medium are [9]

$$\begin{aligned} \nabla^2 E_z - \left(1 - \frac{\varepsilon_{r\parallel}}{\varepsilon_{r\perp}}\right)\frac{\partial^2 E_z}{\partial z^2} + \varepsilon_{r\parallel}k_0^2 E_z = 0 \\ \nabla^2 H_z + \varepsilon_{r\perp}k_0^2 H_z = 0. \end{aligned} \tag{3}$$

Substituting $E_z = E_z(x,y)e^{-jk_z z}$ and $(\partial/\partial x) = 0$, one obtains the following. For the field that is independent of x, where $E_z = A\exp(-j\beta_y y - j\beta_z z)$, one finds β_y

$$\beta_y^2 = k_0^2\varepsilon_{r\parallel} - \frac{\varepsilon_{r\parallel}}{\varepsilon_{r\perp}}k_z^2 = \frac{\varepsilon_{r\parallel}}{\varepsilon_{r\perp}}\left(k_0^2\varepsilon_{r\perp} - k_z^2\right) \tag{4}$$

where k_0 is the wavenumber in vacuum. Substituting into (2) $\nabla_t = -jk_z$ and rewriting these equations for x- and z-components separately, one obtains the following.

x-components

$$\frac{E_{z+}}{d} = \frac{\beta_y^2}{j\omega\varepsilon_\parallel}(H_{x+} + H_{x-})f(\beta_y d) \tag{5a}$$

$$\frac{H_{z+} - H_{z-}}{d} = \frac{-\omega^2\varepsilon_\parallel\mu + k_z^2}{j\omega\mu}E_{x+}f(\beta_y d). \tag{5b}$$

z-components

$$-\frac{E_{x+}}{d} = -j\omega\mu(H_{z+} + H_{z-})f(\beta_y d) \tag{6a}$$

$$-\frac{H_{x+} - H_{x-}}{d} = j\omega\varepsilon_\parallel E_{z+}f(\beta_y d). \tag{6b}$$

One can notice that in (5a) and (6b), only H_x and E_z are present, while in (5b) and (6a), we can find only H_z- and E_x-components. Let us choose equations corresponding to the E_1^y mode, i.e., E_x and H_z are equal to zero and only (5a) and (6b) are nontrivial.

By eliminating H_{x-}, one can obtain

$$2H_{x+} = j\omega\varepsilon_\parallel E_{z+}\frac{2}{\beta_y}\frac{1}{\tan(\beta_y d)}. \tag{7a}$$

For the air layer in Fig. 2, one can similarly write

$$2H_{x+} = -j\omega\varepsilon_0 E_{z+}\frac{2}{\beta_y'}\frac{1}{\tan(\beta_y' d')} \tag{7b}$$

where $\beta_y'^2 = k_0^2 - k_z^2$. The "$-$" sign here comes from the fact that the normal vector points in the opposite direction. When d' goes to infinity, (7b) becomes

$$H_{x+} = j\omega\varepsilon_0 E_{z+}\frac{j}{\beta_y'} \tag{7c}$$

as the propagation constant in the structure in Fig. 2 is larger than that in air and, therefore, β_y' is an imaginary number. Combining (7a) and (7c), one obtains

$$\frac{\varepsilon_{r\parallel}}{\beta_y}\frac{1}{\tan(\beta_y d)} = \frac{j}{\beta_y'}. \tag{8}$$

By introducing $k_y = \beta_y$, $k_{y2} = (\beta_y'/j)$, and $b = 2d$ and using relation $(1/\tan(x)) = \tan((\pi/2) - x)$, an equation similar to "Marcatili's equation" [4], [8] can be obtained as follows:

$$k_y b = \pi + 2\pi n - 2\arctan\left(\frac{1}{\varepsilon_{r\parallel}}\frac{k_y}{k_{y2}}\right) \tag{9}$$

where $n = 0, 1, 2, \ldots, \infty$, $k_y = \sqrt{(\varepsilon_\parallel/\varepsilon_\perp(k_0^2\varepsilon_{r\perp} - k_z^2)}$, $k_{y2} = \sqrt{k_z^2 - k_0^2}$. The case of $n = 0$ corresponds to the E_1^y fundamental mode. To obtain the remaining possible modes (E_z is even with respect to the $y = 0$ plane), one can position the slab onto a magnetic wall.

Regarding the vertical slab, no longitudinal electrical-field component is present for the E_1^y mode; therefore, the "longitudinal" permittivity does not change the second "Marcatili equation" [4]

$$k_x a = \pi m - 2\arctan\left(\frac{k_x}{k_{x3}}\right) \tag{10}$$

where $k_{x3} = \sqrt{k_0^2(\varepsilon_{r\perp} - 1) - k_x^2}$, $m = 1, 2, 3\ldots$.

Thus, the solution procedure can be as follows. Using (9), one can find k_z, then solve (10) for k_x and, eventually, find the correct $k_{z\text{final}}$ as follows:

$$k_{z\text{final}} = \sqrt{k_z^2 - k_x^2}. \tag{11}$$

IV. Result and Discussions

The numerical results are summarized in Fig. 4. Equations (9)–(11) were used to obtain the propagation constant for uniaxial anisotropic waveguides for four combinations of $\varepsilon_{r\perp}$ and $\varepsilon_{r\parallel}$, i.e., 11.56 and 11.56, 11.56 and 9.39, 9.39 and 11.56 (which corresponds to sapphire [10]), and 9.39 and 9.39, respectively.

The wavelength was measured directly at a frequency of 75 GHz by using a movable discontinuity (a rectangular metal "ring") in order to obtain a reference point. The phase values were corrected ($-2\pi n$ correction) to obtain continuous dependence of phase versus frequency. Assuming a constant dielectric waveguide length L, one can write

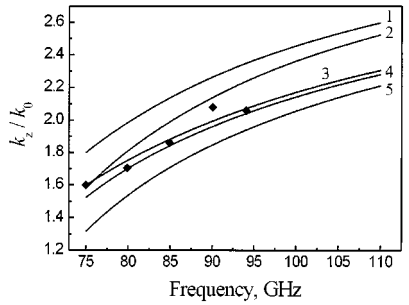

Fig. 4. k_z/k_0 of a DRW made of uniaxial anisotropic materials with cross dimensions of 1.0 × 0.5 mm^2. (1) $\varepsilon_{r\perp} = 11.56, \varepsilon_{r||} = 11.56$. (2) $\varepsilon_{r\perp} = 11.56, \varepsilon_{r||} = 9.39$. (3) Calculated experimental based on the from phase measurement results. (4) $\varepsilon_{r\perp} = 9.39, \varepsilon_{r||} = 11.56$. (5) $\varepsilon_{r\perp} = 9.39, \varepsilon_{r||} = 9.39$; ◇—directly measured experimental points.

$\Delta k = \Delta\phi/L$, where $\Delta\phi$ is the phase-shift change when frequency changes by a small step to the next point, and Δk is a change in the propagation constant in the dielectric waveguide. After obtaining the wavelength at one point by using the phase data, one can calculate the propagation constants at other frequencies (Fig. 4, curve 3). For comparison, the normalized propagation constant measurements were repeated at 80, 85, 90, and 94 GHz. The results are shown in Fig. 4.

One can see in Fig. 4 (curves 3 and 4) that the modified Marcatili method for the sapphire DRW gives a good agreement with the experimental data. The fact that the theoretical curve lies below the experimental one can be explained by the approximative nature of the Marcatili method.

Comparing curve 1 with 2 and 4 with 5, one can see that the anisotropy changes the propagation characteristic considerably. The dispersion is increased, as with curve 2, when $\varepsilon_{||}$ is smaller than $\varepsilon_{\perp}$ or decreased when $\varepsilon_{||}$ is larger than $\varepsilon_{\perp}$, as with curve 4. The latter could be explained as follows. When the frequency is very high, there is almost no longitudinal electric-field component, and the propagation constant results mainly from $\varepsilon_{\perp}$. When the frequency drops, the longitudinal component of the electric field becomes larger; therefore, the effect of larger $\varepsilon_{||}$ becomes stronger and, thus, k_z/k_0 increases. Similarly, one can explain why the dispersion seen in the case of curve 2 is stronger.

V. Conclusion

In this paper, we have presented the modified Marcatili method for the calculation of a rectangular DRW made of uniaxial electrically anisotropic dielectric material with the optical axis coinciding with the axis of the DRW. In a more general case (arbitrary direction of the optical axis, anisotropic permeability, etc.), equations similar to (2) may be derived and solved using this approach. Equations have been derived without guessing the field distribution. This method is relatively simple and sufficiently accurate for a DRW operating far from the cutoff, as with the original Marcatili method for the isotropic case. The propagation constant of an anisotropic sapphire DRW oriented along the optical axis has been measured. Experimental results show a good agreement with those calculated by our approach.

References

[1] A. Sudbø, "Why are the accurate computations of mode fields in rectangular dielectric waveguides difficult?," *J. Lightwave Technol.*, vol. 10, pp. 418–419, Apr. 1992.

[2] T. Itoh, *Numerical Techniques for Microwave and Millimeter-Wave Passive Structures*. New York: Wiley, 1989.

[3] S. Garcia, T. Hung-Bao, R. Martin, and B. Olmedo, "On the application of finite methods in time domain to anisotropic dielectric waveguides," *IEEE Trans. Microwave Theory Tech.*, vol. 44, pp. 2195–2206, Dec. 1996.

[4] E. A. J. Marcatili, "Dielectric rectangular waveguide and directional coupler for integrated optics," *Bell Syst. Tech. J.*, vol. 48, pp. 2071–2102, 1969.

[5] R. M. Knox and P. P. Toulios, "Integrated circuits for the millimeter through optical frequency range," in *Proc. Submillimeter Waves Symp.*, York, NY, 1970, pp. 497–516.

[6] M. I. Oksanen, S. A. Tretyakov, and I. V. Lindell, "Vector circuit theory for isotropic and chiral slabs," *J. Electromagn. Waves Applicat.*, vol. 4, pp. 613–634, 1990.

[7] D. V. Lioubtchenko, S. Dudorov, J. Mallat, J. Tuovinen, and A. V. Räisänen, "Low loss sapphire waveguides for 75–110 GHz frequency range," *IEEE Microwave Wireless Comp. Lett.*, vol. 11, pp. 252–254, June 2001.

[8] T. Itoh, "Dielectric waveguide-type millimeter-wave integrated circuits," in *J. Infrared and Millimeter Waves*, K. J. Button and J. C. Wiltse, Eds. New York: Academic, 1981, vol. 4, ch. 5, pp. 199–273.

[9] Y. Kobayashi and T. Tomohiro, "Resonant modes in shielded uniaxial-anisotropic dielectric rod resonators," *IEEE Trans. Microwave Theory Tech.*, vol. 41, pp. 2198–2205, Dec. 1993.

[10] V. V. Parshin, "Dielectric materials for gyrotron output windows," *Int. J. Infrared Millim. Waves*, vol. 15, pp. 339–348, Feb. 1994.

Microwave I–Q Vector Modulator Using a Simple Technique for Compensation of FET Parasitics

Mitchai Chongcheawchamnan, Sawat Bunnjaweht, David Kpogla, Dongwook Lee, and Ian D. Robertson

***Abstract*—The analysis and design of an improved technique for the realization of vector modulators using analog reflection-type circuits are presented. The analysis focuses on the detrimental effect that the parasitic elements of the FET variable-resistance elements have on the 360° phase and amplitude control. It is shown that a simple circuit technique can be used to compensate for the parasitic effects and achieve a near-ideal constellation. Compared with the balanced structure, the proposed technique leads to a much smaller circuit area and does not require additional complementary control signals. This makes it better suited to commercial wireless applications where low cost is paramount. Simulation and experimental results for an L-band prototype are presented.**

***Index Terms*—Cold FET, parasitic elements, vector modulator.**

I. Introduction

The vector modulator plays an increasingly important role in modern communication systems. For example, in a linearized amplifier system, a vector modulator can provide simultaneous phase and amplitude tuning, rather than applying a variable attenuator cascaded with a variable phase shifter [1]. High-performance vector modulators can be used as the electronic controllable elements for an adaptive beamforming network in phased-array antenna applications [2]. In digital communication applications, a vector modulator is widely

Manuscript received March 26, 2001. This work was supported by the Mahanakorn University of Technology and by RF Hitec Inc.

M. Chongcheawchamnan, S. Bunnjaweht, D. Kpogla, and I. D. Robertson are with the School of Electronic Engineering and Mathematics Department, University of Surrey, Guildford, Surrey, U.K.

D. Lee is with Nextec Microwave and RF Inc., Santa Clara, CA 95050 USA.

Publisher Item Identifier S 0018-9480(02)05215-8.